ACS Energy LETTERS

http://pubs.acs.org/journal/aelccp

Diminishing Space-Charge Layer Effect of Zinc Anodes by an Anion-Immobilized Electrolyte Membrane

Yang Yang,* Haiming Hua, Zeheng Lv, Weiwei Meng, Minghao Zhang, Hang Li, Pengxiang Lin, Jin Yang, Guanhong Chen, Yuanhong Kang, Zhipeng Wen, Jinbao Zhao,* and Cheng Chao Li*

Cite This: *ACS Energy Lett.* 2023, 8, 1959−1968

Read Online

ACCESS | Metrics & More | Article Recommendations | Supporting Information

ABSTRACT: The Zn dendrite issue, which is closely related to the creation of the space-charge region upon local anion depletion during cycling, has plagued the practical applications of aqueous Zn metal batteries (ZMBs). Herein, we propose a Kevlar-derived hydrogel (KevlarH) electrolyte with immobilized anions to diminish the space-charge layer effect. SO_4^{2-} anions are strongly tethered to amide groups of polymer chains, which mitigates the concentration polarization of interfacial Zn^{2+} ions by preventing the anion depletion. Furthermore, the relatively weak interaction between Zn^{2+} cations and carbonyl groups can redistribute Zn^{2+}-ion flux without sacrificing the ion diffusion rate. The synergistic "zincophilic" and "anionphilic" building blocks enable dendrite-free Zn deposition behavior and suppressed side reactions, thereby extending the lifespan of a Zn metal anode up to 3500 h with an ultrahigh Coulombic efficiency of 99.87%. Importantly, the KevlarH electrolyte can be directly used to assemble high-voltage bipolar ZMBs and break the 2 V barrier in aqueous ZMBs.

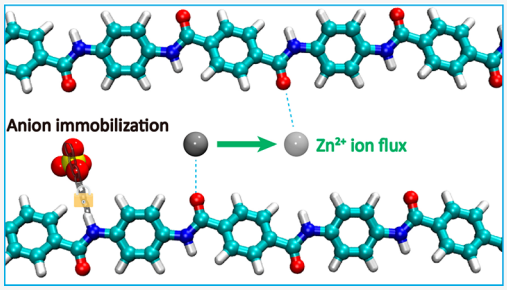

Among various emerging electrochemical energy storage technologies, aqueous zinc metal batteries (AZMBs) based on the fundamentally low-cost element of Zn have stood out for their potential to achieve intrinsic safety, environmental friendliness, and versatility/low requirements for manufacturing processes.[1−3] Despite these prominent advantages, the zinc metal anode still faces severe challenges of dendrite formation and interface parasitic side reactions, including HER (hydrogen evolution reaction) and byproducts generation [such as $Zn_4SO_4(OH)_6{\cdot}xH_2O$ in zinc sulfate solution], that result in poor cycling stability and unsatisfactory Coulombic efficiency (CE) during repeated cycling, which further impede their commercialization.[4−6] Besides, the intrinsic relatively narrow voltage window of water also limits the operating voltage of AZMBs.

To date, numerous efforts have been devoted to resolving the aforementioned issues of the Zn metal anode, such as anode structure design,[7−11] electrolyte regulation,[12−16] separator modification,[17−20] and artificial interface layer construction.[21−25] Despite how these strategies differ from each other, most of them have been predominantly concentrated on manipulating the distribution of Zn^{2+} cations during cycling. It is unquestionable that the homogenized Zn^{2+}-ion flux is prone to smooth and stable Zn deposition behavior. Nonetheless, Zn reduction is a dynamic process that consumes abundant Zn^{2+} ions near the interface in real time; meanwhile, the reversed movement of free anions near the reaction interface exacerbates the Zn^{2+} ion concentration gradient because of the principle of charge neutrality. In 1990, Chazalviel developed an electromigration-limited model to better understand the generation of dendritic electrodeposition of metals.[26] In this theory, anions are expelled from the metal electrode and accumulated near the counter electrode during the metal deposition process, which creates an anion-depleted boundary and electric field at the metal electrode/electrolyte interface. Such a space-charge region is generally accepted to be another important inducement of dendrites formation.[27,28] Accordingly, Archer et al. proposed a novel concept of anion immobilization by introducing ionic liquid−nanoparticle components with tethered anions into liquid electrolytes, and the in-depth theoretical modeling results revealed that immobilizing even a small proportion of anions (10%) would

Received: February 18, 2023
Accepted: March 27, 2023

https://doi.org/10.1021/acsenergylett.3c00385
ACS Energy Lett. 2023, 8, 1959−1968

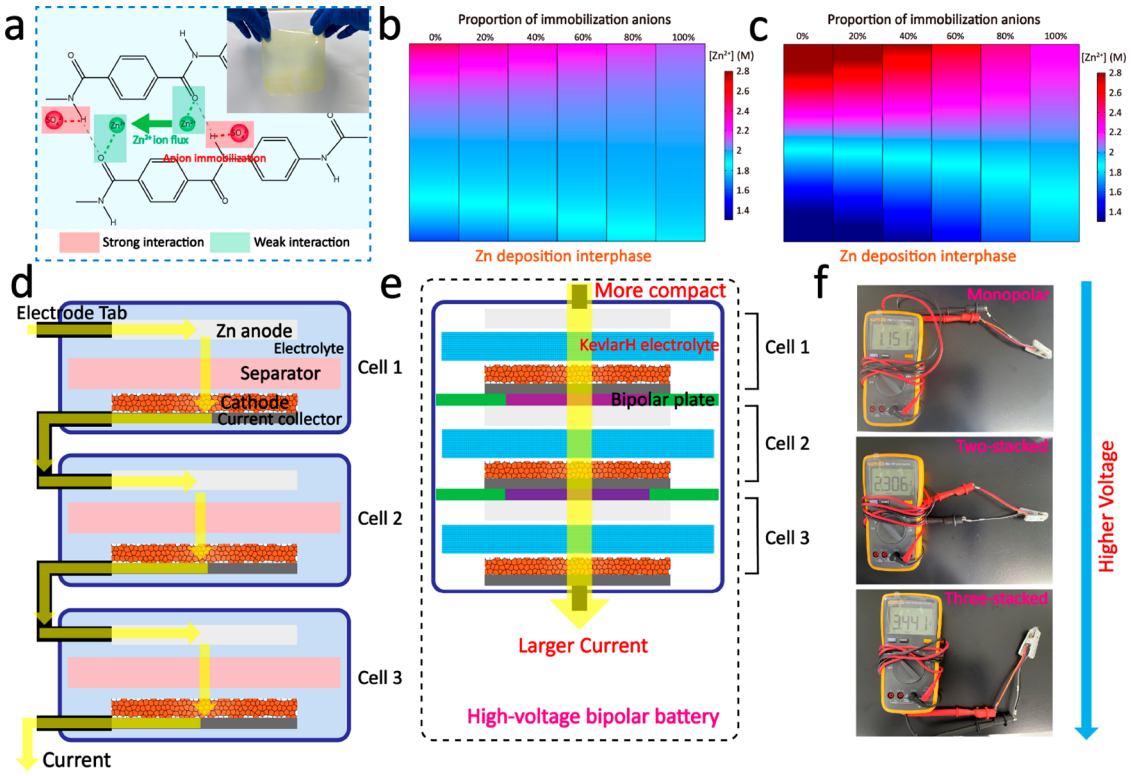

Figure 1. (a) Schemes for structure and Zn^{2+}-conductive mechanism of the KevlarH electrolyte (inset is photograph of the KevlarH electrolyte prepared by the phase inversion method). The distribution of Zn^{2+} concentration from the Zn deposition interphase to the bulk electrolyte with different proportion of immobilization SO_4^{2-} anions (b) after 1.0 s and (c) at the steady state. Schematic representation depicting (d) series-connected conventional monopolar-designed zinc metal batteries (ZMBs) with a liquid electrolyte and (e) the stack of bipolar ZMBs with the KevlarH electrolyte. (f) The open-circuit voltages of bipolar ZMBs with different stack numbers within a sealed cell.

substantially promote the electrodeposition stability.[29,30] To date, the strategy of constructing an anion immobilization interface has become an significant guideline for the suppression of Li dendrite growth.[31−33] Although tethered anionic sites in various organic materials, including Nafion,[34,35] polyanionic polymers,[36,37] and SPEEK,[38,39] have been demonstrated to be coordinated with Zn^{2+} cations to rectify ion transport, the space-charge layer effect induced by free anions in a conventional aqueous electrolyte is usually overlooked.

In this contribution, we propose a Kevlar-derived hydrogel (KevlarH) electrolyte (inset in Figure 1a) with both anion immobilization and cation interaction at the molecular level, which is demonstrated to facilitate a homogeneous flux of Zn^{2+} ions and undermine the space-charge layer effect simultaneously. The strong interaction between amide groups of polymer chains and SO_4^{2-} anions can effectively fix SO_4^{2-} anions, thereby leading to the high transference number of Zn^{2+} and relieving the space-charge effect (Figure 1a). Moreover, the relatively weak interaction between carbonyl groups and Zn^{2+} cations is in favor of redistributing Zn^{2+}-ion flux without sacrificing the ion diffusion rate. Importantly, the gel-state KevlarH electrolyte with good water retention is also demonstrated to be compatible with bipolar battery design.

The superiorities of anion immobilization were first investigated through COMSOL Multiphysics (Figure 1b,c). Because of the creation of a space-charge layer, a serious concentration gradient is observed for the Zn electrode interphase with no immobilization anions after 1.0 s (Figure 1b), and the concentration polarization becomes more significant as the plating process continues to a steady state (Figure 1c). As SO_4^{2-} anions are immobilized, the concentration polarization of interfacial Zn^{2+} ions is well mitigated because it benefits from the diminished space-charge effect. Besides, the gel-state KevlarH electrolyte membrane also provides great opportunities to realize high-voltage bipolar zinc metal battery (ZMB) design.[40] For conventional ZMBs with liquid electrolyte, each single cell is connected in series to form a battery pack (Figure 1d). However, the bipolar ZMB design with a more compact structure impressively reduces the utilization of inert components to improve the energy density (Figure 1e).[41] Moreover, the current in bipolar ZMBs is perpendicular to the electrode plane, which flows directly across the thickness direction of the current collector rather than through its length direction, which leads to the reduced internal resistance and lower ohmic polarization.[42,43] Accordingly, the open-circuit voltages of two- and three-stacked bipolar ZMBs in a single CR-2036-type coin cell case are successfully boosted to 2.306 and 3.411 V (Figure 1f), respectively, thereby demonstrating the feasibility of enhancing the working voltage through the innovative bipolar stacking approach.[44]

The KevlarH electrolyte with the thickness of ~238 μm is prepared through a facile phase inversion process in 2 M $ZnSO_4$ solution (Figure S2), which leads to a interwoven porous structure (Figure S3).[45,46] The energy barrier of cis−trans isomerization for the CO−NH bond ($\Delta E‡$) in poly(*p*-phenylene terephthalamide) (PPTA) is relatively high, reaching 70.6 kJ mol^{-1} (Figure 2a), and the cis conformation energy (ΔE = 22.3 kJ mol^{-1}) is higher than that of the original trans

https://doi.org/10.1021/acsenergylett.3c00385
ACS Energy Lett. 2023, 8, 1959−1968

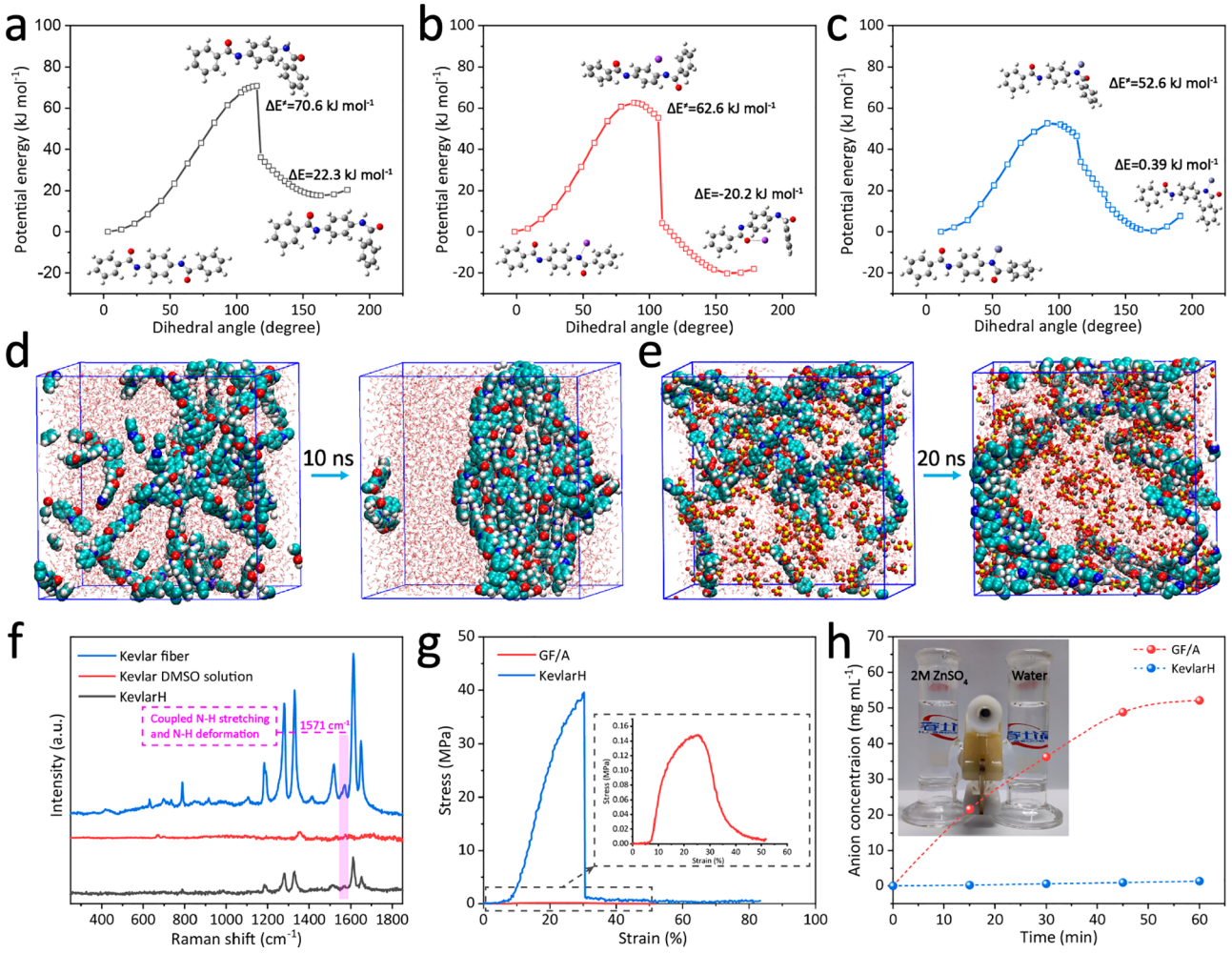

Figure 2. Energy barrier of cis−trans isomerization of CO−NH amide bond in (a) the PPTA molecular chain, (b) the deprotonation of the PPTA molecular chain, and (c) the protonation of the PPTA molecular chain binding with Zn^{2+}. (d) The snapshots of MD simulation for the deprotonation of PPTA molecular chains in water at the original state and after 10 ns. (e) The snapshots of MD simulation for the deprotonation of PPTA molecular chains in $ZnSO_4$ aqueous solution at the original state and after 20 ns. (f) Raman spectra of Kevlar fiber, Kevlar DMSO solution, and KevlarH electrolyte membrane. (g) The measurements of tensile strength for the GF/A separator and KevlarH electrolyte membrane after drying. (h) Concentration diffusion of SO_4^{2-} anions across the GF/A separator and KevlarH electrolyte membrane.

structure, which indicates that PPTA tends to form rigid straight molecular chains. After the deprotonation reaction in KOH/DMSO solution, $\Delta E‡$ is reduced to 62.6 kJ mol^{-1} (Figure 2b), and ΔE is −20.2 kJ mol^{-1}, which is substantially lower than that of the trans, which means that the molecular chains become flexible and are more prone to bending. MD simulations show that after deprotonation, the Kevlar molecular chains are well dispersed in DMSO solution, and the solution remains stable after 20 ns (Figure S4).

When deprotonated PPTA is put into a large amount of water to carry out phase inversion, which is a conventionally used method to prepare Kevlar nanofiber-based hydrogel, protons will recombine to PPTA, which makes PPTA return to the original state of a rigid straight chain. In MD simulation, the PPTA molecular chain gathers into a bundle of fibers after 10 ns (Figure 2d). This compact packing structure implies that the interaction effect between nanofibers and solvent may be relatively weak because of the small specific surface area. However, if the molecular chain is put into $ZnSO_4$ solution instead of pure water, some N atoms will combine with Zn^{2+}. In the combined molecule, $\Delta E‡$ is reduced to 52.6 kJ mol^{-1}, and the energy of the cis and trans conformations are almost equal (Figure 2c), which means that compared with the all-protons-obtained method (in pure water), the phase reversal reaction in $ZnSO_4$ solution provides some bending sites and cross-linking sites for PPTA chains. MD simulation shows that PPTA chains form an interwoven porous structure after 20 ns of simulation (Figure 2e), which enables the KevlarH electrolyte membrane to obtain both high mechanical properties and good water retention. For the Kevlar fiber, Raman peaks between 1183 and 1650 cm^{-1} match well with previously reported results (Table S2).[47] After the deprotonation treatment, most Raman peaks disappear in the Kevlar DMSO solution, which reappears in the KevlarH electrolyte, thereby implying the successful structure reconstruction. It should be noted that the peak intensity of Raman spectra at 1571 cm^{-1} representing the N−H deformation in the KevlarH electrolyte is lower than that of pristine Kevlar fiber (Figure 2f), which reveals that a portion of negatively charged polymer chains may also be integrated with Zn^{2+} and corroborates the theoretical calculation results. As expected, the KevlarH film after drying exhibits outstanding tensile strength (39.6 MPa)

https://doi.org/10.1021/acsenergylett.3c00385
ACS Energy Lett. 2023, 8, 1959−1968

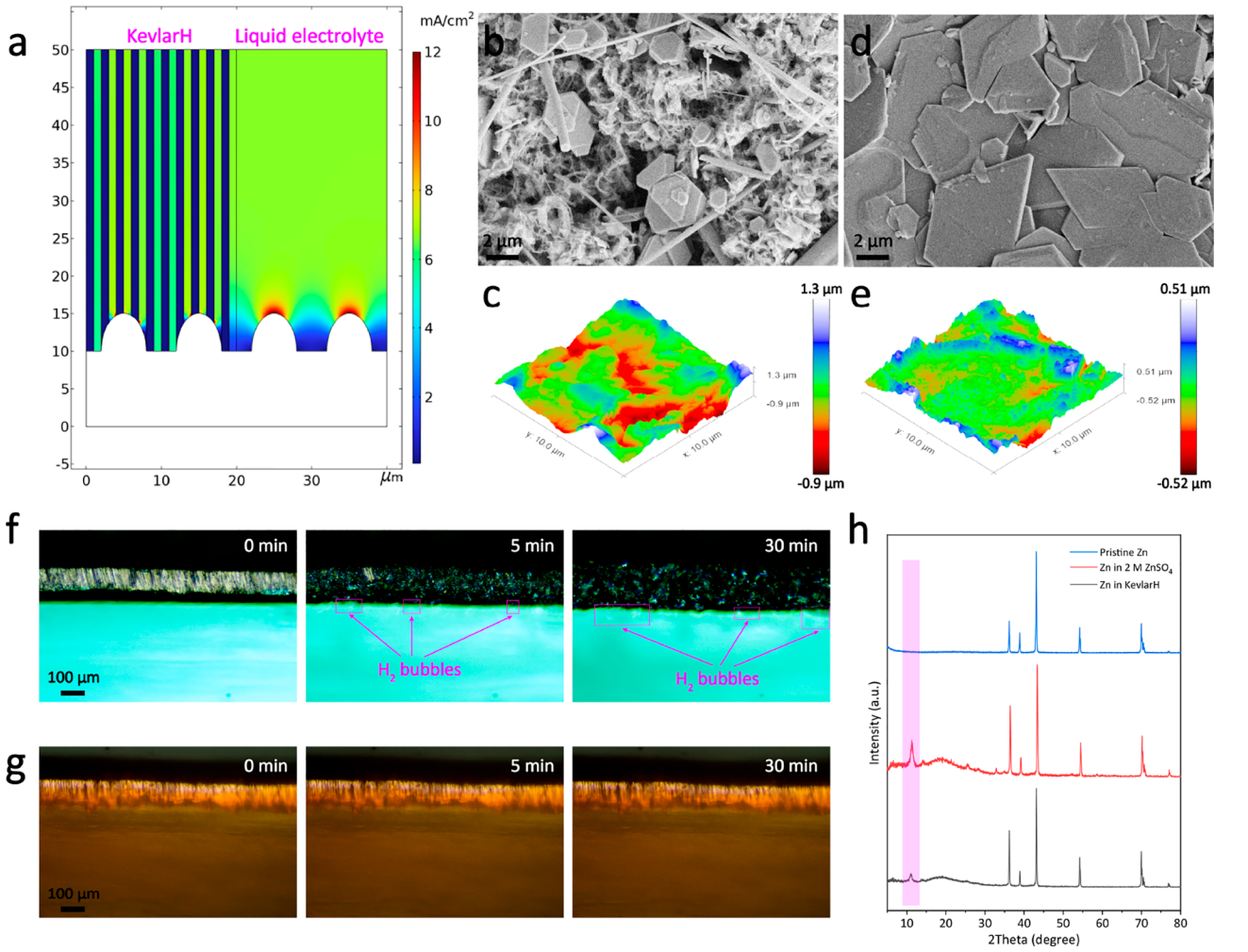

Figure 3. (a) COMSOL Multiphysics modeling of current density distribution in both KevlarH and liquid electrolytes. (b) SEM image and (c) AFM image of Zn electrode after 100 cycles in 2 M $ZnSO_4$ electrolyte. (d) SEM image and (e) AFM image of Zn electrode after 100 cycles in the KevlarH electrolyte. In situ optical images of Zn deposition at 10 mA cm^{-2} in (f) 2 M $ZnSO_4$ electrolyte and (g) the KevlarH electrolyte. (h) XRD patterns of pristine Zn and Zn electrodes after 100 cycles in both electrolytes.

compared with that of commercial GF/A separator (0.15 MPa), thereby ensuring its structural integrity during repeated Zn plating/stripping processes (Figure 2g). Furthermore, the ionic conductivity of KevlarH electrolyte is comparable with conventional 2 M $ZnSO_4$ solution and most gel electrolytes (Figure S5, Table S3). The anion immobilization effect of KelvarH electrolyte was also verified by measuring the transmembrane anion transport property (Figure 2h). The $C_{SO_4^{2-}}$ across the GF/A separator rapidly increases to 21.63 mg mL^{-1} after only 15 min and reaches as high as 52.13 mg mL^{-1} over 60 min. However, the $C_{SO_4^{2-}}$ across the KevlarH electrolyte membrane is maintained lower than 1.35 mg mL^{-1} consistently, thereby indicating the sufficient blocking function to the anion diffusion.

The current density distribution of Zn electrodes in both electrolytes is also simulated (Figure 3a). Aramid nanofibers can serve as fast ion diffusion paths to redistribute Zn-ion flux effectively, and the current density becomes more homogeneous for smooth Zn deposition in the KevlarH electrolyte. After 100 cycles in 2 M $ZnSO_4$ electrolyte, many ultrathin nanosheets with a vertical and loose arrangement are observed, which reveal the formation of Zn dendrites (Figure 3b). In contrast, Zn deposition in the KevlarH electrolyte exhibit a compact stack of microsized horizontal hexagonal plates ranging from 4 to 10 μm (Figure 3d). Moreover, the surface of the Zn electrode after cycling in liquid electrolyte (Figure 3c) is also confirmed to be more rough in contrast than in the case of the KevlarH electrolyte (Figure 3d). Grazing incidence X-ray diffraction (GIXRD) patterns of deposited Zn for different plating times further confirm the preferential orientation of a (002) plane in the KevlarH electrode (Figure S6). Moreover, many hydrogen bubbles are generated continuously on the surface of a Zn electrode in 2 M $ZnSO_4$ during cycling (Figure 3f, Video S1), thereby resulting in dramatic destabilization on the interface. In sharp contrast, no hydrogen bubbles were detected from the Zn electrode in the KevlarH electrolyte (Video S2), thereby indicating the superior interfacial stability (Figure 3g). As shown in Figure 3h, the XRD pattern of the Zn electrode after cycling in the KevlarH electrolyte shows the existence of zinc (JCPDS 01-04-0831) with only weak diffraction peaks of $Zn_4SO_4(OH)_6{\cdot}xH_2O$, which suggests the suppressed side reactions.

The cycling stability of Zn electrodes was investigated by assembling Zn//Zn symmetrical cells. Figure 4a displays the highly reversible electrochemical deposition/stripping behavior for an ultralong lifespan of 3500 h with a stable voltage

https://doi.org/10.1021/acsenergylett.3c00385
ACS Energy Lett. 2023, 8, 1959−1968

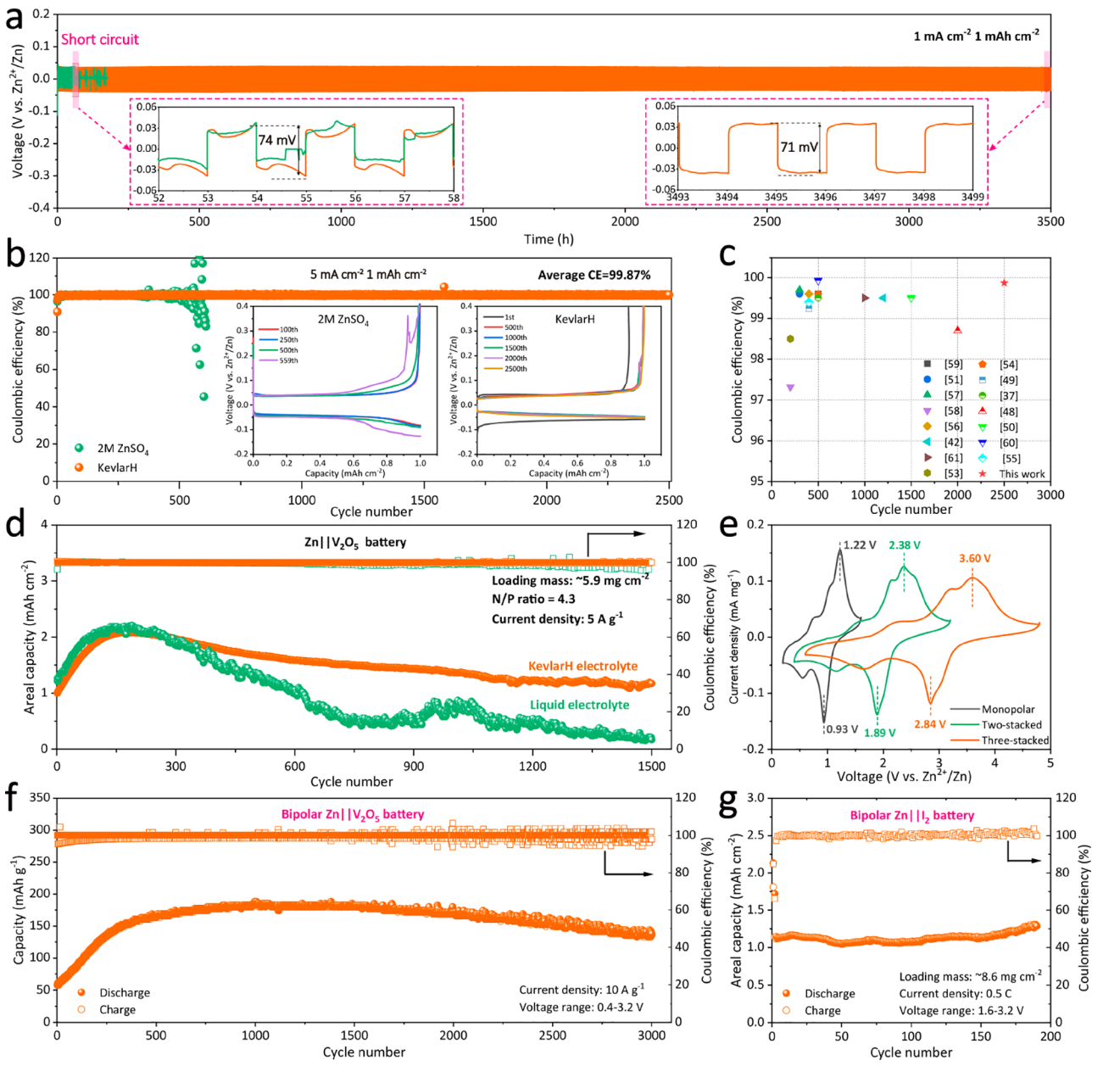

Figure 4. (a) Cycling stability evaluations of Zn//Zn symmetrical cells in 2 M $ZnSO_4$ and KevlarH electrolytes at 1 mA cm^{-2} with a plating/stripping capacity of 1 mAh cm^{-2}. (b) CEs of Zn//Cu half cells in 2 M $ZnSO_4$ and KevlarH electrolytes at 5 mA cm^{-2} with a fixed plating capacity of 1 mAh cm^{-2} (insets are the charge−discharge profiles). (c) The comparison of CEs in different electrolytes. (d) Cycling performance and Coulombic efficiency of Zn||V_2O_5 full batteries in liquid and KevlarH electrolytes at 5 A g^{-1} in the voltage of 0.2−1.6 V. (e) Cyclic voltammetry profiles of Zn||V_2O_5 full batteries at a scan rate of 0.1 mV s^{-1} for the monopolar, two-stacked and three-stacked designs. Cycling performance and Coulombic efficiency of (f) bipolar Zn||V_2O_5 full cells at 10 A g^{-1} and voltages of 0.4−3.2 V and (g) bipolar Zn||I_2 full cells at 0.5 C and the voltages of 1.6−3.2 V.

hysteresis of ∼71 mV at 1 mA cm^{-2} in the KevlarH electrolyte. This is a distinct comparison with the case in 2 M $ZnSO_4$ electrolyte, which showed the internal short-circuit after only 54 h because of the accumulation of Zn dendrites and byproducts in the pores of the GF/A separator (Figure S7). In addition, a prolonged lifespan of 1500 h was also achieved at a high current density of 5 mA cm^{-2} for the KevlarH electrolyte (Figure S8). Besides, the KevlarH electrolyte also delivered an impressive CE improvement (99.87%) over 2500 cycles (Figure 4b), which is superior to most, if not all, recently reported electrolyte regulation studies for Zn metal anodes (Figure 4c).[37,48−61] Inspired by the exceptional Zn deposition/stripping reversibility and interface stability with the KevlarH electrolyte, Zn||V_2O_5 full batteries were fabricated to probe its feasibility in full cells. As shown in Figures 4d and S9, the Zn||V_2O_5 full cell using a thin Zn foil (thickness of 20 μm) with a limited N/P ratio of 4.3 in the KevlarH electrolyte exhibited a high areal capacity of ∼1.2 mAh cm^{-2} after 1500 cycles at 5 A g^{-1} with good interfacial stability (Figure S10), thereby demonstrating a certain predominance over the routine liquid electrolyte. Self-discharge tests (Figure S11) showed that the capacity retention of the Zn||V_2O_5 full cell with the KevlarH electrolyte (95.0%) was also superior to that of the routine liquid electrolyte (82.3%).

https://doi.org/10.1021/acsenergylett.3c00385
ACS Energy Lett. 2023, 8, 1959−1968

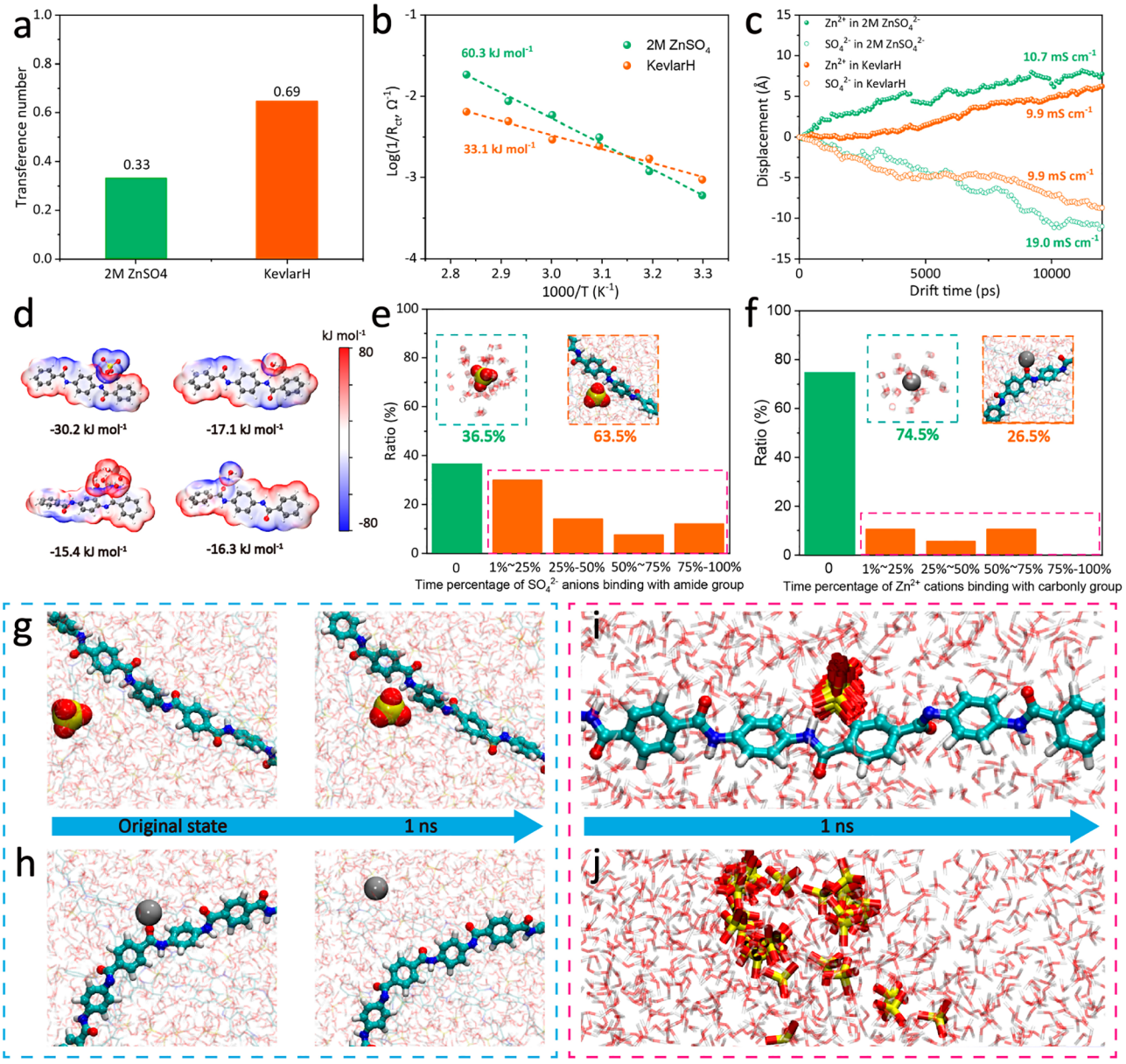

Figure 5. (a) Transference numbers and (b) desolvation activation energy of Zn electrodes in 2 M $ZnSO_4$ and KevlarH electrolytes. (c) Conductivity calculations of 2 M $ZnSO_4$ and KevlarH electrolytes from MDs. (d) MESP isosurface plots between an aramid chain and different species of Zn^{2+}, SO_4^{2-}, and H_2O. The ratio of various binding conditions between (e) SO_4^{2-} anions and an amide group and (f) Zn^{2+} cations and a carbonyl group. Structural snapshots from MD simulations of (g) a free SO_4^{2-} anion interacting with an aramid polymer chain and (h) a Zn^{2+} interacting with an aramid polymer chain transport to the free state. (i) Statistical trajectory analysis of a SO_4^{2-} anion binding with an aramid polymer chain. (j) Statistical trajectory analysis of a SO_4^{2-} anion in 2 M $ZnSO_4$.

Furthermore, the two-stacked and three-stacked bipolar Zn||V_2O_5 batteries were further assembled with the KevlarH electrolyte, which show reduction peaks of 1.89 and 2.84 V and oxidation peaks of 2.38 and 3.60 V, respectively (Figure 4e). These values were nearly twice and three times higher (0.93 and 1.22 V, respectively) than the value of a conventional monopolar Zn||V_2O_5 cell, thereby verifying that the successful fabrication of bipolar batteries in a single coin cell case without ionic shortcut can enhance the output voltage of batteries effectively. Encouragingly, the two-stacked bipolar Zn||V_2O_5 cell delivers a high reversible capacity of 138.4 mAh g^{-1} after 3000 cycles at 10 A g^{-1} in the expanded voltage range of 0.4–3.2 V (Figure 4f). In addition, the electrochemical performance of a three-stacked bipolar Zn||V_2O_5 cell in the voltage range of 0.6–4.8 V was also investigated (Figure S12). Moreover, the two-stacked bipolar Zn||I_2 full cell using the KevlarH electrolyte also showed a high areal capacity of ∼1.30 mAh cm^{-2} after 200 cycles at 0.5 C with a negligible capacity decay (Figure 4g), thereby suggesting the universality of KevlarH electrolyte for bipolar ZMB systems.

The interface stability should be closely associated with the Zn^{2+} transport and charge-transfer kinetics. As shown in Figures 5a and S13, the Zn^{2+} transference number ($t_{Zn^{2+}}$) of the KevlarH electrolyte (0.69) was measured to be higher than that of the liquid electrolyte (0.33). It reveals that a higher proportion of Zn^{2+} ions is involved in efficient migration in the KevlarH electrolyte, which is attributed to the anion immobilization effect. As shown in Figures 5b and S14, the

https://doi.org/10.1021/acsenergylett.3c00385
ACS Energy Lett. 2023, 8, 1959−1968

desolvation activation energy (E_a) of KevlarH electrolyte (33.1 kJ mol^{-1}) is also calculated to be smaller than that of liquid electrolyte (60.3 kJ mol^{-1}), which implies that coordinated H_2O molecules in $[Zn^{2+}(H_2O)_6]$ may interact with Kevlar nanofibers to reduce the energy barrier of removing the solvation sheath.

Molecular dynamic (MD) simulations were performed to get deeper insight into the species distribution and interaction in both electrolytes (Figure S15). As shown in Figure 5c, the ionic conductivities of 2 M $ZnSO_4$ KevlarH electrolytes were calculated to be 29.7 and 19.8 mS cm^{-1}, respectively, which are basically consistent with the measured experimental results (44.0 and 35.6 mS cm^{-1}, respectively). Moreover, cationic and anionic contributions to the total current can be further analyzed. It is evident that the anionic conductivity of the KevlarH electrolyte (9.9 mS cm^{-1}) is substantially reduced compared with that of 2 M $ZnSO_4$ (19.0 mS cm^{-1}), thereby demonstrating the contributing anion immobilization impact. However, the cationic conductivity of the KevlarH electrolyte (9.9 mS cm^{-1}) is still close to that of 2 M $ZnSO_4$ (10.7 mS cm^{-1}), which implies the relatively weak interaction between aramid nanofibers and Zn^{2+}.

More quantized interaction energies between different species and aramid chains are shown in Figure 5d. As expected, the binding free energy between SO_4^{2-} ions and the amide group of the aramid chain (−30.2 kJ mol^{-1}) is higher than in the case between the hydrated Zn^{2+} ions and the carbonyl group of the aramid chain (−15.4 kJ mol^{-1}). Furthermore, both the amide and carbonyl groups can form hydrogen bonds with water molecules to effectively reduce the amount of free water, which show binding energies of −17.1 and −16.3 kJ mol^{-1}, respectively. Despite the huge amount of SO_4^{2-} anions in the KevlarH electrolyte, only 36.5% of SO_4^{2-} anions have no interaction with aramid chains, which indicates that the proportion of immobilization anions is as high as 63.5% (Figure 5e). Notably, about 12% of SO_4^{2-} anions are completely fixed to the aramid during the overall simulation duration of 20 ns. By contrast, the interactions between Zn^{2+} cations and aramid chains are transient dynamic processes that contribute to no irreversible fixation of the Zn^{2+} cation (Figure 5f). Once a SO_4^{2-} anion approaches the amide group of the aramid polymer chain, it is spontaneously absorbed onto the surface of the aramid nanofiber (Figure 5g and Video S3). Moreover, the corresponding statistical trajectory analysis during the duration of 1 ns indicates the strong immobilization effect of the SO_4^{2-} anion without obvious movement (Figure 5i), whereas the random thermal motion of a SO_4^{2-} anion in 2 M $ZnSO_4$ is detected (Figure 5j). In addition, the interaction between the Zn^{2+} cation and aramid chain is modest, which ensures the fast separation of Zn^{2+} ions from binding sites (Figure 5h, Video S4) and is in favor of redistributing Zn^{2+}-ion flux without sacrificing the ion diffusion rate.

Through comprehensive experimental and theoretical investigations, the simultaneous cation interaction and anion immobilization are confirmed in the KevlarH electrolyte, which originates from the weak interaction between carbonyl groups and Zn^{2+} cations and the strong interaction between amide groups and SO_4^{2-} anions, respectively. Importantly, the KevlarH electrolyte membrane can be directly used to fabricate bipolar zinc metal batteries, which not only reduce inert components but also enhance the output voltage in a single cell case. The KevarH electrolyte provides a facile pathway for realizing a long-life and ultrastable Zn metal anode, thereby enabling the development of high-voltage bipolar ZMBs.

■ ASSOCIATED CONTENT

Supporting Information

The Supporting Information is available free of charge at https://pubs.acs.org/doi/10.1021/acsenergylett.3c00385.

Experimental section, theoretical calculation methods, and supplementary figures and tables (PDF)

Video S1: Zn deposition behavior in liquid electrolyte (MP4)

Video S2: Zn deposition behavior in the KevlarH electrolyte (MP4)

Video S3: Dynamic snapshots of MD simulations of a free SO_4^{2-} anion interacting with an aramide polymer chain (MP4)

Video S4: Dynamic snapshots of MD simulations of a Zn^{2+} cation interacting with an aramide polymer chain (MP4)

■ AUTHOR INFORMATION

Corresponding Authors

Yang Yang − *State Key Lab of Physical Chemistry of Solid Surfaces, State-Province Joint Engineering Laboratory of Power Source Technology for New Energy Vehicle, College of Chemistry and Chemical Engineering, Xiamen University, Xiamen 361005, P. R. China;* orcid.org/0000-0003-4215-5767; Email: yangyang419@xmu.edu.cn

Jinbao Zhao − *State Key Lab of Physical Chemistry of Solid Surfaces, State-Province Joint Engineering Laboratory of Power Source Technology for New Energy Vehicle, College of Chemistry and Chemical Engineering, Xiamen University, Xiamen 361005, P. R. China;* orcid.org/0000-0002-2753-7508; Email: jbzhao@xmu.edu.cn

Cheng Chao Li − *School of Chemical Engineering and Light Industry, Guangdong University of Technology, Guangzhou 510006, P. R. China;* orcid.org/0000-0003-2434-760X; Email: licc@gdut.edu.cn

Authors

Haiming Hua − *State Key Lab of Physical Chemistry of Solid Surfaces, State-Province Joint Engineering Laboratory of Power Source Technology for New Energy Vehicle, College of Chemistry and Chemical Engineering, Xiamen University, Xiamen 361005, P. R. China*

Zeheng Lv − *State Key Lab of Physical Chemistry of Solid Surfaces, State-Province Joint Engineering Laboratory of Power Source Technology for New Energy Vehicle, College of Chemistry and Chemical Engineering, Xiamen University, Xiamen 361005, P. R. China*

Weiwei Meng − *State Key Laboratory of Vanadium and Titanium Resources Comprehensive Utilization, Panzhihua 617000, P. R. China*

Minghao Zhang − *State Key Lab of Physical Chemistry of Solid Surfaces, State-Province Joint Engineering Laboratory of Power Source Technology for New Energy Vehicle, College of Chemistry and Chemical Engineering, Xiamen University, Xiamen 361005, P. R. China*

Hang Li − *State Key Lab of Physical Chemistry of Solid Surfaces, State-Province Joint Engineering Laboratory of Power Source Technology for New Energy Vehicle, College of*

https://doi.org/10.1021/acsenergylett.3c00385
ACS Energy Lett. 2023, 8, 1959−1968

Chemistry and Chemical Engineering, Xiamen University, Xiamen 361005, P. R. China

Pengxiang Lin − *State Key Lab of Physical Chemistry of Solid Surfaces, State-Province Joint Engineering Laboratory of Power Source Technology for New Energy Vehicle, College of Chemistry and Chemical Engineering, Xiamen University, Xiamen 361005, P. R. China*

Jin Yang − *State Key Lab of Physical Chemistry of Solid Surfaces, State-Province Joint Engineering Laboratory of Power Source Technology for New Energy Vehicle, College of Chemistry and Chemical Engineering, Xiamen University, Xiamen 361005, P. R. China*

Guanhong Chen − *State Key Lab of Physical Chemistry of Solid Surfaces, State-Province Joint Engineering Laboratory of Power Source Technology for New Energy Vehicle, College of Chemistry and Chemical Engineering, Xiamen University, Xiamen 361005, P. R. China*

Yuanhong Kang − *State Key Lab of Physical Chemistry of Solid Surfaces, State-Province Joint Engineering Laboratory of Power Source Technology for New Energy Vehicle, College of Chemistry and Chemical Engineering, Xiamen University, Xiamen 361005, P. R. China*

Zhipeng Wen − *School of Chemical Engineering and Light Industry, Guangdong University of Technology, Guangzhou 510006, P. R. China*

Complete contact information is available at: https://pubs.acs.org/10.1021/acsenergylett.3c00385

Notes

The authors declare no competing financial interest.

■ ACKNOWLEDGMENTS

This work is supported by the National Natural Science Foundation of China (22109030 and 22021001), the Fundamental Research Funds for the Central Universities (20720220073), the Key Research and Development Program of Yunnan Province (202103AA080019), the Fujian Industrial Technology Development and Application Plan (2022I0002), and the Guangdong Basic and Applied Basic Research Foundation (2021A1515010177). The authors acknowledge Beijng PARATERA Tech Co., Ltd. for providing HPC resources that have contributed to the research results reported within this paper (https://paratera.com/).

■ REFERENCES

(1) Wu, M. L.; Zhang, Y.; Xu, L.; Yang, C. P.; Hong, M.; Cui, M. J.; Clifford, B. C.; He, S. M.; Jing, S. S.; Yao, Y.; Hu, L. B. A sustainable chitosan-zinc electrolyte for high-rate zinc-metal batteries. *Matter* **2022**, *5*, 3402−3416.

(2) Pan, H.; Shao, Y.; Yan, P.; Cheng, Y.; Han, K. S.; Nie, Z.; Wang, C.; Yang, J.; Li, X.; Bhattacharya, P.; Mueller, K. T.; Liu, J. Reversible aqueous zinc/manganese oxide energy storage from conversion reactions. *Nat. Energy* **2016**, *1*, 16039.

(3) Chen, X.; Ruan, P.; Wu, X.; Liang, S; Zhou, J. Crystal Structures, Reaction Mechanisms, and Optimization Strategies of MnO2 Cathode for Aqueous Rechargeable Zinc Batteries. *Acta Phys.-Chim. Sin.* **2022**, *38*, 2111003.

(4) Qiu, H. Y.; Du, X. F.; Zhao, J. W.; Wang, Y. T.; Ju, J. W.; Chen, Z.; Hu, Z. L.; Yan, D. P.; Zhou, X. H.; Cui, G. L. Zinc anode-compatible in-situ solid electrolyte interphase via cation solvation modulation. *Nat. Commun.* **2019**, *10*, 5374.

(5) Su, J. R.; Yin, X. X.; Zhao, H. N.; Yang, H. J.; Yang, D.; He, L.; Wang, M. L.; Jin, S. R.; Zhao, K. N.; Wang, Y. Z.; Wei, Y. J. Temperature-Dependent Nucleation and Electrochemical Performance of Zn Metal Anodes. *Nano Lett.* **2022**, *22*, 1549−1556.

(6) Zheng, J.; Zhao, Q.; Tang, T.; Yin, J.; Quilty, C. D.; Renderos, G. D.; Liu, X.; Deng, Y.; Wang, L.; Bock, D. C.; Jaye, C.; Zhang, D.; Takeuchi, E. S.; Takeuchi, K. J.; Marschilok, A. C.; Archer, L. A. Reversible epitaxial electrodeposition of metals in battery anodes. *Science* **2019**, *366*, 645−648.

(7) Xie, F. X.; Li, H.; Wang, X. S.; Zhi, X.; Chao, D. L.; Davey, K.; Qiao, S. Z. Mechanism for Zincophilic Sites on Zinc-Metal Anode Hosts in Aqueous Batteries. *Adv. Energy Mater.* **2021**, *11*, 2003419.

(8) Yuksel, R.; Buyukcakir, O.; Seong, W. K.; Ruoff, R. S. Metal-Organic Framework Integrated Anodes for Aqueous Zinc-Ion Batteries. *Adv. Energy Mater.* **2020**, *10*, 1904215.

(9) Xu, Z. X.; Li, M.; Sun, W. Y.; Tang, T.; Lu, J.; Wang, X. L. An Ultrafast, Durable, and High-Loading Polymer Anode for Aqueous Zinc-Ion Batteries and Supercapacitors. *Adv. Mater.* **2022**, *34*, 2200077.

(10) Wang, Z.; Huang, J. H.; Guo, Z. W.; Dong, X. L.; Liu, Y.; Wang, Y. G.; Xia, Y. Y. A Metal-Organic Framework Host for Highly Reversible Dendrite-free Zinc Metal Anodes. *Joule* **2019**, *3*, 1289−1300.

(11) Li, C.; Xie, X.; Liu, H.; Wang, P.; Deng, C.; Lu, B.; Zhou, J.; Liang, S. Integrated 'all-in-one' strategy to stabilize zinc anodes for high-performance zinc-ion batteries. *Natl. Sci. Rev.* **2022**, *9*, nwab177.

(12) Patil, N.; de la Cruz, C.; Ciurduc, D.; Mavrandonakis, A.; Palma, J.; Marcilla, R. An Ultrahigh Performance Zinc-Organic Battery using Poly(catechol) Cathode in Zn(TFSI)(2)-Based Concentrated Aqueous Electrolytes. *Adv. Energy Mater.* **2021**, *11*, 2100939.

(13) Huang, C.; Zhao, X.; Liu, S.; Hao, Y. S.; Tang, Q. L.; Hu, A. P.; Liu, Z. X.; Chen, X. H. Stabilizing Zinc Anodes by Regulating the Electrical Double Layer with Saccharin Anions. *Adv. Mater.* **2021**, *33*, 2100445.

(14) Meng, R. W.; Li, H.; Lu, Z. Y.; Zhang, C.; Wang, Z. X.; Liu, Y. X.; Wang, W. C.; Ling, G. W.; Kang, F. Y.; Yang, Q. H. Tuning Zn-Ion Solvation Chemistry with Chelating Ligands toward Stable Aqueous Zn Anodes. *Adv. Mater.* **2022**, *34*, 2200677.

(15) Li, C.; Shyamsunder, A.; Hoane, A. G.; Long, D. M.; Kwok, C. Y.; Kotula, P. G.; Zavadil, K. R.; Gewirth, A. A.; Nazar, L. F. Highly reversible Zn anode with a practical areal capacity enabled by a sustainable electrolyte and superacid interfacial chemistry. *Joule* **2022**, *6*, 1103−1120.

(16) Jin, S.; Yin, J. F.; Gao, X. S.; Sharma, A.; Chen, P. Y.; Hong, S. F.; Zhao, Q.; Zheng, J. X.; Deng, Y.; Joo, Y. L.; Archer, L. A. Production of fast-charge Zn-based aqueous batteries via interfacial adsorption of ion-oligomer complexes. *Nat. Commun.* **2022**, *13*, 2283.

(17) Li, C.; Sun, Z. T.; Yang, T.; Yu, L. H.; Wei, N.; Tian, Z. N.; Cai, J. S.; Lv, J. Z.; Shao, Y. L.; Rummeli, M. H.; Sun, J. Y.; Liu, Z. F. Directly Grown Vertical Graphene Carpets as Janus Separators toward Stabilized Zn Metal Anodes. *Adv. Mater.* **2020**, *32*, 2003425.

(18) Yang, H. J.; Qiao, Y.; Chang, Z.; Deng, H.; He, P.; Zhou, H. S. A Metal-Organic Framework as a Multifunctional Ionic Sieve Membrane for Long-Life Aqueous Zinc-Iodide Batteries. *Adv. Mater.* **2020**, *32*, 2004240.

(19) Zhang, X. T.; Li, J. X.; Qi, K. W.; Yang, Y. Q.; Liu, D. Y.; Wang, T. Q.; Liang, S. Q.; Lu, B. A.; Zhu, Y. C.; Zhou, J. An Ion-Sieving Janus Separator toward Planar Electrodeposition for Deeply Rechargeable Zn-Metal Anodes. *Adv. Mater.* **2022**, *34*, 2205175.

(20) Song, Y.; Ruan, P.; Mao, C.; Chang, Y.; Wang, L.; Dai, L.; Zhou, P.; Lu, B.; Zhou, J.; He, Z. Metal−Organic Frameworks Functionalized Separators for Robust Aqueous Zinc-Ion Batteries. *Nano-Micro Lett.* **2022**, *14*, 218.

(21) Kang, L. T.; Cui, M. W.; Jiang, F. Y.; Gao, Y. F.; Luo, H. J.; Liu, J. J.; Liang, W.; Zhi, C. Y. Nanoporous CaCO3 Coatings Enabled Uniform Zn Stripping/Plating for Long-Life Zinc Rechargeable Aqueous Batteries. *Adv. Energy Mater.* **2018**, *8*, 1801090.

(22) Liu, Q.; Wang, Y.; Hong, X. D.; Zhou, R.; Hou, Z.; Zhang, B. A. Elastomer-Alginate Interface for High-Power and High-Energy Zn Metal Anodes. *Adv. Energy Mater.* **2022**, *12*, 2200318.

(23) Guo, R. T.; Liu, X.; Xia, F. J.; Jiang, Y. L.; Zhang, H. Z.; Huang, M.; Niu, C. J.; Wu, J. S.; Zhao, Y.; Wang, X. P.; Han, C. H.; Mai, L. Q. Large-Scale Integration of a Zinc Metasilicate Interface Layer Guiding Well-Regulated Zn Deposition. *Adv. Mater.* **2022**, *34*, 2202188.
(24) Guo, Z. K.; Fan, L. S.; Zhao, C. Y.; Chen, A. S.; Liu, N. N.; Zhang, Y.; Zhang, N. Q. A Dynamic and Self-Adapting Interface Coating for Stable Zn-Metal Anodes. *Adv. Mater.* **2022**, *34*, 2105133.
(25) Yang, J. L.; Li, J.; Zhao, J. W.; Liu, K.; Yang, P. H.; Fan, H. J. Stable Zinc Anodes Enabled by a Zincophilic Polyanionic Hydrogel Layer. *Adv. Mater.* **2022**, *34*, 2202382.
(26) Chazalviel, J. N. Electrochemical aspects of the generation of ramified metallic electrodeposits. *Phys. Rev. A* **1990**, *42*, 7355−7367.
(27) Chang, H. J.; Ilott, A. J.; Trease, N. M.; Mohammadi, M.; Jerschow, A.; Grey, C. P. Correlating Microstructural Lithium Metal Growth with Electrolyte Salt Depletion in Lithium Batteries Using 7Li MRI. *J. Am. Chem. Soc.* **2015**, *137*, 15209−15216.
(28) Bai, P.; Li, J.; Brushett, F. R.; Bazant, M. Z. Transition of lithium growth mechanisms in liquid electrolytes. *Energy Environ. Sci.* **2016**, *9*, 3221−3229.
(29) Tikekar, M. D.; Archer, L. A.; Koch, D. L. Stability Analysis of Electrodeposition across a Structured Electrolyte with Immobilized Anions. *J. Electrochem. Soc.* **2014**, *161*, A847.
(30) Lu, Y.; Korf, K.; Kambe, Y.; Tu, Z.; Archer, L. A. Ionic-Liquid−Nanoparticle Hybrid Electrolytes: Applications in Lithium Metal Batteries. *Angew. Chem.* **2014**, *53*, 488−492.
(31) Zhao, C.-Z.; Zhang, X.-Q.; Cheng, X.-B.; Zhang, R.; Xu, R.; Chen, P.-Y.; Peng, H.-J.; Huang, J.-Q.; Zhang, Q. An anion-immobilized composite electrolyte for dendrite-free lithium metal anodes. *Proc. Natl. Acad. Sci. U. S. A.* **2017**, *114*, 11069−11074.
(32) Zhang, W.; Zhuang, H. L.; Fan, L.; Gao, L.; Lu, Y. A "cation-anion regulation" synergistic anode host for dendrite-free lithium metal batteries. *Sci. Adv.* **2018**, *4*, eaar4410.
(33) Li, Y.; Liu, Y.; Xue, L.; Chen, W.; Lei, T.; Hu, A.; Huang, J.; Wang, X.; Wang, X.; Chen, B.; Hu, Y.; Yang, C.; Xiong, J. Eliminating anion depletion region and promoting Li+ solvation via anionphilic metal organic framework for dendrite-free lithium deposition. *Nano Energy* **2022**, *92*, 106708.
(34) Cui, Y.; Zhao, Q.; Wu, X.; Chen, X.; Yang, J.; Wang, Y.; Qin, R.; Ding, S.; Song, Y.; Wu, J.; Yang, K.; Wang, Z.; Mei, Z.; Song, Z.; Wu, H.; Jiang, Z.; Qian, G.; Yang, L.; Pan, F. An Interface-Bridged Organic−Inorganic Layer that Suppresses Dendrite Formation and Side Reactions for Ultra-Long-Life Aqueous Zinc Metal Anodes. *Angew. Chem.* **2020**, *59*, 16594−16601.
(35) Wang, S.; Yang, Z.; Chen, B.; Zhou, H.; Wan, S.; Hu, L.; Qiu, M.; Qie, L.; Yu, Y. A highly reversible, dendrite-free zinc metal anodes enabled by a dual-layered interface. *Energy Storage Mater.* **2022**, *47*, 491−499.
(36) Yang, J.-L.; Li, J.; Zhao, J.-W.; Liu, K.; Yang, P.; Fan, H. J. Stable Zinc Anodes Enabled by a Zincophilic Polyanionic Hydrogel Layer. *Adv. Mater.* **2022**, *34*, 2202382.
(37) Lin, P.; Cong, J.; Li, J.; Zhang, M.; Lai, P.; Zeng, J.; Yang, Y.; Zhao, J. Achieving ultra-long lifespan Zn metal anodes by manipulating desolvation effect and Zn deposition orientation in a multiple cross-linked hydrogel electrolyte. *Energy Storage Mater.* **2022**, *49*, 172−180.
(38) He, X.; Cui, Y.; Qian, Y.; Wu, Y.; Ling, H.; Zhang, H.; Kong, X.-Y.; Zhao, Y.; Xue, M.; Jiang, L.; Wen, L. Anion Concentration Gradient-Assisted Construction of a Solid−Electrolyte Interphase for a Stable Zinc Metal Anode at High Rates. *J. Am. Chem. Soc.* **2022**, *144*, 11168−11177.
(39) Fan, H.; Wang, M.; Yin, Y.; Liu, Q.; Tang, B.; Sun, G.; Wang, E.; Li, X. Tailoring interfacial Zn2+ coordination via a robust cation conductive film enables high performance zinc metal battery. *Energy Storage Mater.* **2022**, *49*, 380−389.
(40) Kim, S.-H.; Kim, J.-H.; Cho, S.-J.; Lee, S.-Y. All-Solid-State Printed Bipolar Li−S Batteries. *Adv. Energy Mater.* **2019**, *9*, 1901841.
(41) Homann, G.; Meister, P.; Stolz, L.; Brinkmann, J. P.; Kulisch, J.; Adermann, T.; Winter, M.; Kasnatscheew, J. High-Voltage All-Solid-State Lithium Battery with Sulfide-Based Electrolyte: Challenges for the Construction of a Bipolar Multicell Stack and How to Overcome Them. *ACS Appl. Energy Mater.* **2020**, *3*, 3162−3168.
(42) Lin, Z.; Mao, M.; Yue, J.; Liu, B.; Wu, C.; Suo, L.; Hu, Y.-S.; Li, H.; Huang, X.; Chen, L. Wearable Bipolar Rechargeable Aluminum Battery. *ACS Mater. Lett.* **2020**, *2*, 808−813.
(43) Liu, T.; Yuan, Y.; Tao, X.; Lin, Z.; Lu, J. Bipolar Electrodes for Next-Generation Rechargeable Batteries. *Adv. Sci.* **2020**, *7*, 2001207.
(44) Cao, D.; Sun, X.; Wang, Y.; Zhu, H. Bipolar stackings high voltage and high cell level energy density sulfide based all-solid-state batteries. *Energy Storage Mater.* **2022**, *48*, 458−465.
(45) Yang, M.; Cao, K.; Sui, L.; Qi, Y.; Zhu, J.; Waas, A.; Arruda, E. M.; Kieffer, J.; Thouless, M. D.; Kotov, N. A. Dispersions of Aramid Nanofibers: A New Nanoscale Building Block. *ACS Nano* **2011**, *5*, 6945−6954.
(46) Zhu, J.; Yang, M.; Emre, A.; Bahng, J. H.; Xu, L.; Yeom, J.; Yeom, B.; Kim, Y.; Johnson, K.; Green, P.; Kotov, N. A. Branched Aramid Nanofibers. *Angew. Chem.* **2017**, *56*, 11744−11748.
(47) Yang, B.; Wang, L.; Zhang, M.; Luo, J.; Ding, X. Timesaving, High-Efficiency Approaches To Fabricate Aramid Nanofibers. *ACS Nano* **2019**, *13*, 7886−7897.
(48) Yang, F.; Hua, H.; Lai, P.; Lin, P.; Yang, J.; Zhang, M.; Yang, Y.; Zhao, J. Synergetic Modulation of Ion Flux and Water Activity in a Single Zn2+ Conductor Hydrogel Electrolyte for Ultrastable Aqueous Zinc-Ion Batteries. *ACS Appl. Energy Mater.* **2022**, *5*, 10872−10882.
(49) Miao, L.; Wang, R.; Di, S.; Qian, Z.; Zhang, L.; Xin, W.; Liu, M.; Zhu, Z.; Chu, S.; Du, Y.; Zhang, N. Aqueous Electrolytes with Hydrophobic Organic Cosolvents for Stabilizing Zinc Metal Anodes. *ACS Nano* **2022**, *16*, 9667−9678.
(50) Jin, Y.; Han, K. S.; Shao, Y.; Sushko, M. L.; Xiao, J.; Pan, H.; Liu, J. Stabilizing Zinc Anode Reactions by Polyethylene Oxide Polymer in Mild Aqueous Electrolytes. *Adv. Funct. Mater.* **2020**, *30*, 2003932.
(51) Nie, X.; Miao, L.; Yuan, W.; Ma, G.; Di, S.; Wang, Y.; Shen, S.; Zhang, N. Cholinium Cations Enable Highly Compact and Dendrite-Free Zn Metal Anodes in Aqueous Electrolytes. *Adv. Funct. Mater.* **2022**, *32*, 2203905.
(52) Yang, J. H.; Zhang, Y.; Li, Z. L.; Xu, X.; Su, X. Y.; Lai, J. W.; Liu, Y.; Ding, K.; Chen, L. Y.; Cai, Y. P.; Zheng, Q. F. Three Birds with One Stone: Tetramethylurea as Electrolyte Additive for Highly Reversible Zn-Metal Anode. *Adv. Funct. Mater.* **2022**, *32*, 2209642.
(53) Meng, R.; Li, H.; Lu, Z.; Zhang, C.; Wang, Z.; Liu, Y.; Wang, W.; Ling, G.; Kang, F.; Yang, Q.-H. Tuning Zn-Ion Solvation Chemistry with Chelating Ligands toward Stable Aqueous Zn Anodes. *Adv. Mater.* **2022**, *34*, 2200677.
(54) Yang, M.; Zhu, J.; Bi, S.; Wang, R.; Niu, Z. A Binary Hydrate-Melt Electrolyte with Acetate-Oriented Cross-Linking Solvation Shells for Stable Zinc Anodes. *Adv. Mater.* **2022**, *34*, 2201744.
(55) Zeng, X.; Mao, J.; Hao, J.; Liu, J.; Liu, S.; Wang, Z.; Wang, Y.; Zhang, S.; Zheng, T.; Liu, J.; Rao, P.; Guo, Z. Electrolyte Design for In Situ Construction of Highly Zn2+-Conductive Solid Electrolyte Interphase to Enable High-Performance Aqueous Zn-Ion Batteries under Practical Conditions. *Adv. Mater.* **2021**, *33*, 2007416.
(56) Hao, Y.; Feng, D. D.; Hou, L.; Li, T. Y.; Jiao, Y. C.; Wu, P. Y. Gel Electrolyte Constructing Zn (002) Deposition Crystal Plane Toward Highly Stable Zn Anode. *Adv. Sci.* **2022**, *9*, 2104832.
(57) Zhang, C.; Shin, W.; Zhu, L.; Chen, C.; Neuefeind, J. C.; Xu, Y.; Allec, S. I.; Liu, C.; Wei, Z.; Daniyar, A.; Jiang, J.-X.; Fang, C.; Alex Greaney, P.; Ji, X. The electrolyte comprising more robust water and superhalides transforms Zn-metal anode reversibly and dendrite-free. *Carbon Energy* **2021**, *3*, 339−348.
(58) Wu, C.; Sun, C.; Ren, K.; Yang, F.; Du, Y.; Gu, X.; Wang, Q.; Lai, C. 2-methyl imidazole electrolyte additive enabling ultra-stable Zn anode. *Chem. Eng. J.* **2023**, *452*, 139465.
(59) Zhang, Y.; Huang, Z.; Wu, K.; Yu, F.; Zhu, M.; Wang, G.; Xu, G.; Wu, M.; Liu, H.-K.; Dou, S.-X.; Wu, C. 2D anionic nanosheet additive for stable Zn metal anodes in aqueous electrolyte. *Chem. Eng. J.* **2022**, *430*, 133042.

https://doi.org/10.1021/acsenergylett.3c00385
ACS Energy Lett. 2023, 8, 1959−1968

(60) Ming, F.; Zhu, Y.; Huang, G.; Emwas, A.-H.; Liang, H.; Cui, Y.; Alshareef, H. N. Co-Solvent Electrolyte Engineering for Stable Anode-Free Zinc Metal Batteries. *J. Am. Chem. Soc.* **2022**, *144*, 7160−7170.
(61) Jin, S.; Duan, F.; Wu, X.; Li, J.; Dan, X.; Yin, X.; Zhao, K.; Wei, Y.; Sui, Y.; Du, F.; Wang, Y. Stabilizing Interface pH by Mixing Electrolytes for High-Performance Aqueous Zn Metal Batteries. *Small* **2022**, *18*, 2205462.

https://doi.org/10.1021/acsenergylett.3c00385
ACS Energy Lett. 2023, 8, 1959−1968